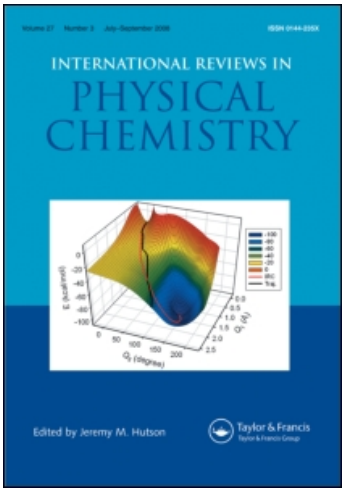

International Reviews in Physical Chemistry
Publication details, including instructions for authors and subscription information:
http://www.informaworld.com/smpp/title~content=t713724383

Experimental characterization and computational simulation of chemical reaction dynamics

Pamela M. Aker[a]; James J. Valentini[b]
[a] Department of Chemistry, University of Pittsburgh, Pittsburgh, PA, USA [b] Department of Chemistry, Columbia University, New York, NY, USA

To cite this Article Aker, Pamela M. and Valentini, James J.(1993) 'Experimental characterization and computational simulation of chemical reaction dynamics', International Reviews in Physical Chemistry, 12: 2, 363 — 390
To link to this Article: DOI: 10.1080/01442359309353286
URL: http://dx.doi.org/10.1080/01442359309353286

INTERNATIONAL REVIEWS IN PHYSICAL CHEMISTRY, 1993, VOL. 12, NO. 2, 363–390

Experimental characterization and computational simulation of chemical reaction dynamics

A case study

by PAMELA M. AKER

Department of Chemistry, University of Pittsburgh, Pittsburgh, PA 15213, USA

and JAMES J. VALENTINI

Department of Chemistry, Columbia University, New York, NY 10027, USA

We present an examination of the $H+HX \rightarrow H_2+X$ and $H+HX \rightarrow HX+H$ (X = Cl, Br, I) reactions as a case study of the kind of detailed dynamical information that can be provided by combining thorough experimental measurements with extensive theoretical (computational) simulations. The experimental component is state-to-state dynamics measurement of the absolute cross-sections for reaction from specific quantum states of the HX reactant molecule to particular quantum states of the H_2 and HX product molecules. The interpretation of the quite detailed experimental results is provided by the theoretical component of this work, computational simulations of the reaction dynamics using quasi-classical trajectory calculations. Testing and validation of the quasi-classical trajectory calculations is done by comparison of the state-to-state dynamics theoretically predicted with the dynamics actually revealed in the experiments. When the trajectory calculations are so validated they are used to explore aspects of the dynamics not accessible experimentally and to develop physical models that promote understanding of the dynamics.

1. Introduction

One of the goals of chemical physics is to provide first principles description of the way chemical reactions take place. By this we mean to describe the reactions in terms of the quantum mechanical motion of atoms on a potential energy surface that expresses the chemical interaction among the atoms. Such a description would be easy were it possible to observe the atoms going about the business of reacting, but such observation is problematic. The uncertainty principle imposes significant fundamental barriers to observing the atoms moving along the potential energy surface, while the rapidity with which reactants are converted to products adds practical barriers on top of these. For example, for the reactions examined here, the $H+HX \rightarrow H_2+X$ and $H+HX \rightarrow HX+H$ (X = Cl, Br, I) reactions, the time during which reactants are transformed into products is only about 10 femtoseconds.

Faced with the difficulty of directly observing the transformation of reactants to products, some physical chemists concede to nature the upper hand here and devise experiments to reveal indirectly the details of the reactant-to-product transformation. One major indirect approach to elucidating the intimate dynamics of reaction is experimental state-to-state dynamics, in which the reactants are prepared in a specific quantum state and the cross-sections for reaction into specific quantum states of the

0144-235X/93 $10·00

products are measured. State-to-state dynamics aims to infer the mechanism of the reactant-to-product transformation from clues contained in the identities of the quantum states of the products formed from specific quantum states of the reactants. These quantum-state-to-quantum-state couplings are clues because they are determined by the path the reactants take over the potential energy surface in getting to products. The couplings are only clues, not direct, obvious information, because no single part of the path determines any particular state-to-state coupling; rather the interactions experienced in the entire path are accumulated and expressed in all the couplings.

Inference is thus an essential part of extracting from state-to-state measurements the desired information about the reaction dynamics. As with any kind of inference, a model is developed and relied upon to connect the observations with the underlying molecular behaviour. The ambiguity is that different models containing different molecular dynamics can predict the same observations, and the lack of a single-valued inference from the observations to the dynamics limits the interpretation of experimental state-to-state results.

The solution is to complement the experimental measurements with theoretical calculations that describe the transformation of reactants to products—the motion of the atoms on the potential energy surface connecting reactants with products—in terms of first principles. In fact, it might seem possible to dispense with the experiments entirely, and just employ quantum chemistry to compute the potential energy surface and quantum reaction dynamics to carry out the reactant-to-product transformation on this computed surface. Were this possible, it is exactly the way one would characterize chemical reactions.

However, the computation of the potential energy surface for any reaction system involving elements beyond the second row of the periodic table or a system with more than four or five atoms of any type is quite difficult. Consider that even for very simple chemical reactions the potential energy surface is of very high dimensionality. For example, for $H+CH_4 \rightarrow H_2+CH_3$ the potential energy surface is 12-dimensional, and the energy of interaction for many geometrical configurations of the atoms along each of the 12 dimensions must be calculated to cover all the configurations explored during the course of a reaction. If one could get by with a calculation of the potential energy surface for just five values along each of the 12 dimensions one would still need a quantum calculation of the electronic energy for more than one-half million geometrical configurations. Add to this the fact that for a realistic representation of the reaction dynamics a potential energy surface globally accurate to about 0·04 eV (1 kcal mol^{-1}) is needed, and the challenge of producing an *ab initio* surface for anything but the simplest reactions becomes apparent.

Even if a globally accurate *ab initio* potential can be produced, exact quantum dynamical calculations on it are computationally daunting. For example, for the $H+CH_4 \rightarrow H_2+CH_3$ reaction at any reasonable energy above that required to surmount the barrier between reactants and products, about 0·5 eV, there are many thousands of coupled channels that must be included and converged in the calculations in order to get chemically accurate results. Methodological developments and increasing speeds of computers will put more and more complex reactions within reach of exact quantum calculation, yet the general treatment of reaction dynamics by exact quantum calculation is some time away.

There remains consequently a place for state-to-state dynamics experiments and a need for approximate, but more tractable, theoretical calculations to provide their

interpretation. Approximations in determining the potential energy surface and in projecting the system from reactants to products will in general be necessary. In contrast to exact quantum calculations, the accuracy of approximate calculations cannot be assessed without experimental tests, and the calculations cannot be reliably used to explore and characterize the dynamics of real molecular systems without validation by complementary experimental measurements. Experimental state-to-state dynamics can provide these critical tests of approximate calculations. If the accuracy of the calculations is verified by comparison with the state-to-state experimental results, the calculations can be be used with some confidence to expore the reaction dynamics more completely than experiment alone would allow.

This is precisely the approach we have taken and will illustrate it here by case study of the $H+HX \rightarrow H_2+X$ and $H+HX \rightarrow HX+H$ ($X=Cl$, Br, I) reactions. The computational method we have chosen to simulate the transformation of reactants to products is quasi-classical trajectory (QCT) calculations (Truhlar and Muckerman 1979, Raff and Thompson 1985). In QCT calculations the classical equations of motion govern the approach of the reactants, their transformation into products, and the separation of the products. However, since the calculations have to make contact with experimental results that describe the reactions in terms of the coupling of quantum states of reactants with quantum states of products, the calculations cannot be purely classical, and they are not. Rather, the starting points for the trajectories are selected from a distribution of energies, momenta, and positions that is dictated by quantum mechanics, and at the completion of the trajectory the energies and momenta of the products are assigned quantum numbers by associating them with the quantum states that have energies and momenta closest to those of the classically treated products.

For the $H+HX \rightarrow H_2+X$ and $H+HX \rightarrow HX+H$ ($X=Cl$, Br, I) reactions that serve as a case study here the potential energy surfaces on which the classical dynamics is followed are derived by semi-empirical approaches (Baer and Last 1981, Schwenke *et al.* 1989). Since we are the consumers, not the producers, of such surfaces we will say little here about their construction. The only aspect of these surfaces that concerns us is their accuracy, and this will be judged empirically by the agreement of the results of dynamics calculations done on them with corresponding experimental measurements.

The computations play an even more significant role than we have so far admitted, because the experimental studies only approximate the ideal of state-to-state dynamics. The ideal experiment would prepare each of the two reactants in a single quantum state and arrange for them to collide at a single (delta function) relative energy. Such experiments are conceivable but not achievable, for they dictate experimental conditions so restrictive as to make the experiments prohibitively difficult. Rather, all state-to-state dynamics experiments approximate this ideal, starting with at least some distribution over the quantum states of the reactants and examining collisions at some finite range of relative energies. But how much information is lost in so relaxing the standards of the experiment? Is some important aspect of the dynamics obscured by the averaging over quantum states or relative energies? The calculations, which can be carried out easily for any single quantum state and relative energy or any distribution over quantum states and spread in energies, provide a means to answer these questions.

2. The case study—collisions of $H+HX$($X=Cl$, Br, I)

2.1. *Chemical, energetic, and kinematic properties*

The molecular reaction system we have chosen to present here as an example of the successful marriage of experimental state-to-state dynamics and computational

simulation of reaction dynamics is the H + HX series, where HX is a hydrogen halide, HCl, HBr, or HI. This system has several attractive features. First, there are three possible chemical outcomes of the collision of an H atom with a hydrogen halide HX:

abstraction of the H atom,

$$H' + HX(v,j) \rightarrow H'H(v', j') + X, \tag{1}$$

exchange of the hydrogen atoms,

$$H' + HX(v, j) \rightarrow H'X(v', j') + H, \tag{2}$$

and the inelastic (non-reactive) energy transfer process,

$$H' + HX(v,j) \rightarrow HX(v', j') + H'. \tag{3}$$

Here we have labelled one of the hydrogen atoms with a prime to distinguish processes (2) and (3), and (v,j) and (v',j') indicate the rotational and vibrational quantum numbers of, respectively, the reactants and products in the state-to-state measurements. Characterizing the competition among different pathways invests the state-to-state experimental measurements with additional information, and provides more points of contact between the theoretical calculations and the experimental results.

Second, the energetics of the reactions, the thermochemistry and reaction energy barriers, systematically vary over the series. For the abstraction channel the reaction with HCl is nearly thermoneutral, while that with HBr is mildly exoergic, and that with HI substantially exoergic. The quantitative details are presented in table 1. The abstraction reaction energetic barriers, which can only be calculated (Baer and Last 1981, Schwenke *et al.* 1989), not measured, follow the thermochemistry, with the H + HCl having a substantial barrier and H + HI having almost no barrier at all. For the exchange reactions (see table 2) the trend in barrier heights (Baer and Last, 1981, Schwenke *et al.* 1989) is similar but weaker—all three reactions have substantial

Table 1. Energetics of the $H + HX \rightarrow H_2 + X$ reactions. All energies are given in eV.

Hydrogen halide	ΔH	$E_b(\theta = 180°)^a$	$\langle E_b(\theta) \sin\theta \rangle^b$
HCl	−0·05	0·22	0·86
HBr	−0·72	0·08	0·53
HI	−1·42	0·03	0·30

[a] Collinear barrier heights, from Baer and Last (1981).
[b] Weighted average of the barrier height over the range $\theta = 180°$ to $\theta = 90°$, computed using data from Baer and Last (1981).

Table 2. Energetics of the $H' + HX \rightarrow H'X + H$ reactions. All energies are given in eV.

Hydrogen halide	ΔH	$E_b(\theta = 180°)^a$	$\langle E_b(\theta) \sin\theta \rangle^b$
HCl	0·0	0·54	1·17
HBr	0·0	0·48	1·00
HI	0·0	0·42	0·82

[a] Collinear barrier heights, from Baer and Last (1981).
[b] Weighted average of the barrier height over the range $\theta = 180°$ to $\theta = 90°$, computed using data from Baer and Last (1981).

barriers—but since the products and reactants are chemically identical all are exactly thermoneutral. These energy trends help in identifying the key dynamical features evidenced in the state-to-state results.

Finally, in this homologous series of reactions the kinematics, that is the mass effects are essentially constant. The dynamics of the reactions depend only on the relative masses, the reduced masses, not the total mass of all the atoms involved, and in this reaction series the reduced masses of the reactants, $\mu_{\text{reactants}} = m_H m_{HX}/(m_H + m_{HX})$, and of the products, $\mu_{\text{products}} = m_{H_2} m_X/(m_{H_2} + m_X)$, are very little affected by the mass of X. Since for all X $m_X \gg m_H$, the value of $\mu_{\text{reactants}}$ in all three cases is very close to m_H, 0·97, 0·99, and 0·99 amu to be specific, while μ_{products} is nearly m_{H_2}, 1·89, 1·95, and 1·97 amu. This kinematic uniformity among the reactions affords the possibility of identifying those aspects of the reaction dynamics that are determined by or strongly influenced by the kinematics.

These reactions have a rich history in reaction dynamics. Among the previous studies are crossed molecular beam differential cross-section measurements of the exchange reactions, $D + HX$, at moderate ($\approx$0·4 eV) collision energy (McDonald and Herschbach 1975, Bauer *et al.* 1978). Cadman and Polanyi (1968) and Cadman *et al.* (1967) have observed small yields of the excited I atom [$I(^2P_{1/2})$] in the $H + HI \rightarrow H_2 + I$ reaction. Vibrational excitation of the HCl was shown to enhance the cross-section for the D + HCl exchange reaction by Arnoldi and Wolfrum (1976). More recently Wight *et al.* (1984) used i.r. fluorescence measurements to characterize the vibrational energy flow in H(D) + HCl(DCl) exchange and inelastic collisions and Cousins and Leone (1987) did the same for the H(D) + HF system. Closest to the experiments reviewed here are the state-to-state dynamics measurements of Kliner *et al.* (1991) on the $H + HI \rightarrow H_2 + I$ reaction, which we discuss in Section 3.

Numerous theoretical calculations on these systems have also been reported. Many of these were undertaken because of the prototypical light + light-heavy kinematics of that the reactions epitomize. The theoretical work is too extensive to discuss here, and most of it is not directly connected to issues dealt with in this paper, so we will mention only a few examples. However, the interested reader is referred to the comprehensive review by Clary and Henshaw (1986) for a thorough discussion. Of the previous theoretical calculations perhaps closest to the results described here are QCT calculations by Schatz (1987) on inelastic and reactive exchange dynamics in high energy H + HF collisions. Baer (1972) and Baer and Kouri (1972) have discussed the rotational product distributions that are likely to arise in these reactions. Three-dimensional close coupling calculations for the $H + HBr \rightarrow HBr + H$ reaction have been reported by Clary (1985).

2.2. *The experiments*

State-to-state dynamics experiments require three key ingredients: (1) reactant preparation, (2) reaction under single-collision conditions to make sure that only the reactants in the prepared states can react, and (3) product detection, with quantum state specificity. These three elements are provided in our experiments by using nanosecond-duration laser pulses both for reactant preparation and for spectroscopic detection of the product states. Such short pulse lengths permit the attainment of single-collision conditions, defined as conditions permitting only one collision of the prepared reactants and no collisions of any products formed before the products are detected. Since typical collision velocities are 10^5–10^6 cm s^{-1}, reactant pressures of a few Torr or less yield single-collision conditions on the nanosecond time scale.

Given the significant barrier heights in the $H + HCl \rightarrow H_2 + Cl$ abstraction reaction, and in all three exchange reactions, a comprehensive study of this series has to be done at collision energies substantially in excess of typical laboratory thermal energies. Consequently, we have investigated these reactions at collision energies of 1·3 and 1·6 eV, using photolysis of HI to generate H atom reactants with the requisite translational energy. The photolysis is effected by a u.v. pulsed laser, with a wavelength of 266 nm or 280 nm. One complication encountered here is that at 266 nm the photolysis of HI leads to two different H atom translational energies, since there are two photodissociation channels, $H + I(^2P_{3/2})$ and $H + I(^2P_{1/2})$, with quantum yields of 0·75 and 0·25 (Clear *et al.* 1975, Schmiedl *et al.* 1982). The spin–orbit excited electronic state of the I atom, $(^2P_{1/2})$, lies 0·942 eV above the $(^2P_{3/2})$ ground state, so the two H atom translational energies are substantially different, 1·6 eV and 0·7 eV. For photolysis at 280 nm only the $H + I(^2P_{3/2})$ fragment channel is active, and only a single H atom translational energy, 1·3 eV is produced.

Even though the energy of the photons effecting the photolysis is very well defined, the $H + HX$ collision energy has some spread, due to the 300 K thermal motion of the HI before photolysis and the 300 K thermal motion of the HX reactant (Van der Zande *et al.* 1991). However, the masses of the HX reactant and the HI that serves as the H atom photolytic precursor are both much greater than the mass of the H atom, so their thermal velocities and velocity spreads are much smaller than the velocity of the photolytic H atom. Consequently, the thermal motions produce collision energies with spreads of only 0·05 to 0·1 eV, much smaller than the mean collision energies of 0·7 to 1·6 eV, and the collision energy is reasonably well specified.

Except for selecting the relative energy, there is no state preparation in these state-to-state experiments, for very little is needed. The high frequency vibrations of the hydrogen halides dictate that at room temperature the populations of all excited vibrational states are vanishingly small, so our reactants all have $v = 0$. There is a measurable Boltzmann distribution over HX rotational states, but only about a half-dozen states are significantly populated, and the effect of rotational state on the reactions at these hyperthermal relative energies is expected to be small. However, as mentioned in the Introduction this is one of those aspects of the non-ideal experiment whose dynamical significance can be addressed in the QCT calculations. Although we will not discuss it here, the QCT results bear out the expectation that the effect of changing the reactant j is very small for these reactions at these high collision energies.

Several different product species are involved in these experiments, HCl, HBr, HI, and H_2, so we need in the experiments a spectroscopic technique for quantum-state-resolved detection of the products that possesses some generality. This we provide by coherent anti-Stokes Raman scattering (CARS) spectroscopy. CARS is a four-wave mixing process that exploits the existence of Raman resonances in the third-order optical hyperpolarizability (Valentini 1985). All molecules have at least one Raman active vibrational mode that makes their detection by CARS possible, and in particular all diatomic molecules have Raman-active vibrations. As a light scattering technique CARS has a time resolution limited only by the duration of the laser pulses used to effect it, so establishing single-collision detection conditions is straightforward.

A complete description of the experimental apparatus, with a full consideration of all the elements critical to its operation, is provided in several of our previous publications (Aker *et al.* 1989, 1992) and the interested reader is referred to these for complete details.

2.3. *The calculations*

Our QCT calculations used an algorithm and code developed by Muckerman (1989). The time step in the integration of the classical equations of motion was varied to achieve adequate energy conservation. The calculations for each system (H + HCl, H + HBr, and H + HI) consisted of several thousand trajectories run for each reactant v, j state, with the j's chosen according to the 300 K Boltzmann distribution characterizing the experiments. The collision energies for the calculations were chosen to be the most probable collision energies of the experiments, 1·6 and 0·7, or 1·3 eV. Since the collision energy spread in the experiments is small (see discussion above) we did not attempt to run calculations over a range of energies around these most probable values.

For the H + HCl system the trajectories were run on a potential energy surface described by an extended LEPS-3C function calculated by Schwenke *et al.* (1989), while for the H + HBr calculations a simple LEPS function with parameters given by Parr and Kuppermann (1989) was used. In our calculations on H + HI we tried two different surfaces, a LEPS surface computed by Parr and Kuppermann (1989) and a DIM-3C surface originating with Baer and Last (1981) and subsequently modified by Clary (1989). Lists of the parameters needed to define these surfaces are tabulated in a previous publication (Aker and Valentini 1990), which also presents a more detailed discussion of them.

3. $H + HX \rightarrow H_2 + X$ (X = Cl, Br, I)

Using the experimental techniques described in the previous Section, we measured partial and total reaction cross-sections for the $H + HX \rightarrow H_2 + X$ abstraction reactions (Aker *et al.* 1989, 1992). Some of the results of these measurements are presented in figures 1–4. For all the results shown the collision energy was nominally 1·6 eV, but as discussed in Section 2 the production of 1·6 eV H atoms by HI photolysis at 266 nm also yields some H atoms, giving $H + HX$ collisions with 0·7 eV collision energy. Relative vibrational and rotational state distributions for $H + HI \rightarrow H_2 + I$ were subsequently reported by Kliner *et al.* (1991) using the same experimental approach, but with multiphoton ionization (MPI) instead of CARS product detection. The results of that experiment nicely corroborate our earlier measurements.

Our H_2 project vibrational state distributions are shown in fig. 1. These H_2 product vibrational distributions vary significantly with halogen atom identity and hence reaction energetics (see table 1). In the $H + HCl \rightarrow H_2 + Cl$ reaction the measured vibrational distribution monotonically and strongly decreases: $P(v'=0:1) = 0{\cdot}92(4):0{\cdot}08(1)$ giving $\langle v' \rangle$ of 0·08. (Here and elsewhere in this paper the number contained in parentheses following a numerical quantity gives the uncertainty in the least significant digit of the numerical quantity.) The $H + HI \rightarrow H_2 + I$ reaction in contrast produces a vibrational distribution that is strongly inverted: $P(v'=0:1:2:3:4) = 0{\cdot}27(7):0{\cdot}46(7):0{\cdot}21(5):0{\cdot}05(3):0{\cdot}01(1)$, with $\langle v' \rangle$ of 1·1. The vibrational energy disposal in the $H + HBr \rightarrow H_2 + Br$ reaction is intermediate between these two extremes, in fact the $P(v'=0:1:2) = 0{\cdot}65(3):0{\cdot}30(3):0{\cdot}05(1)$, and $\langle v' \rangle = 0{\cdot}4$, are almost exactly the mean of the other two distributions.

The H_2 rotational state distributions measured also show strong variance with halogen atom identity. Figure 2 presents a plot of these distributions measured for the $H + HCl \rightarrow H_2 + Cl$ reaction, while figures 3 and 4 are the analogous results for the H + HBr and H + HI reactions. These results show that the rotational state distribution shifts to higher j' as the reaction exoergicity increases. For example, the maximum

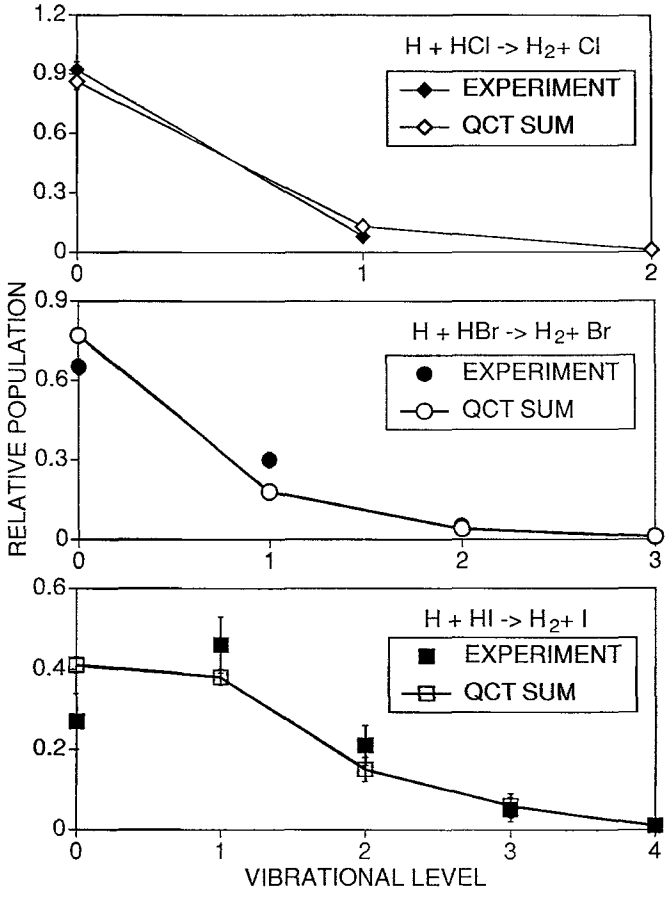

Figure 1. Vibrational state distributions for the H_2 product of the $H+HX \rightarrow H_2+X$ reactions at 1·6 eV collision energy.

observed j' level $v'=0$ is 11, 13, and 17 for $X=$Cl, Br, and I, respectively, and the peaks of the distributions, and $\langle j' \rangle$ also increase, with the latter being 6, 8, and 13, respectively.

How do we understand and interpret such detailed results? Given only the experimental data we try to formulate a phenomenological model that will reproduce them. That is exactly what we did. We proposed that an adaptation of the Franck–Condon model for reactions (Schatz and Ross 1977) could explain the observed energy disposal in the $H+HX \rightarrow H_2+X$ abstraction reactions. In its original implementation, the Franck–Condon model assumed that reaction can be thought of as a sudden transition from reactants to products, occurring in a small region of coordinate space located at the saddle point, the region where the reactant kinetic energy has been expended climbing the barrier separating reactants from products. However, in our $H+HX \rightarrow H_2+X$ reactions the reactant kinetic energy will be totally expended only when the system hits the inner corner of the potential energy surface at small H–H and H–X separations, since the collision energy is decidedly larger than the barrier height.

We reasoned that if a sudden transition from reactants to products occurs in this region of coordinate space the H_2 would be born with a vibrational state distribution

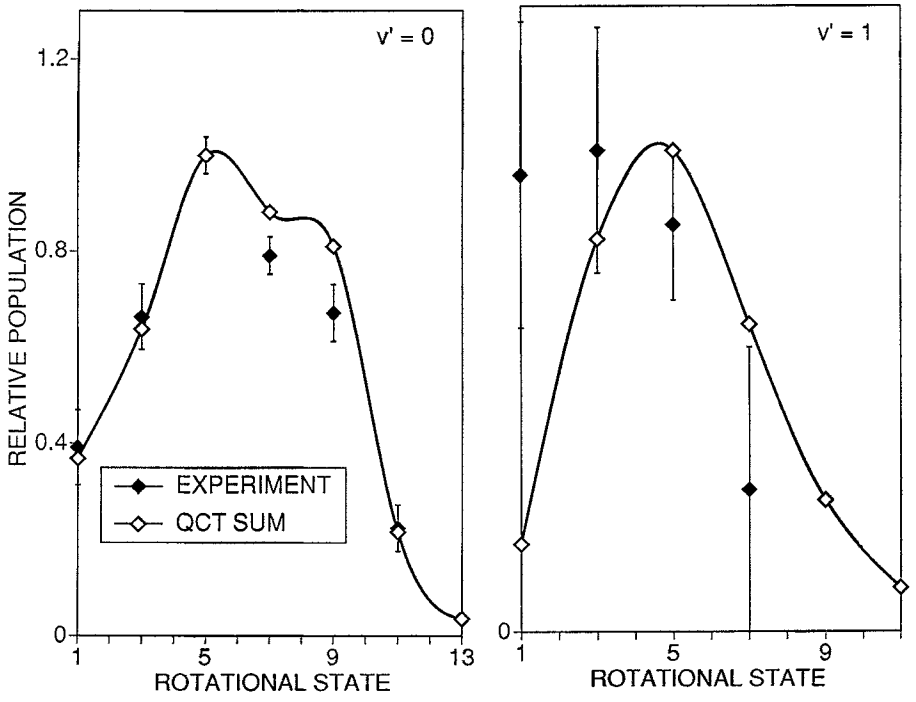

Figure 2. Rotational state distributions for the H_2 product of the $H + HCl \rightarrow H_2 + Cl$ reaction at 1·6 eV collision energy.

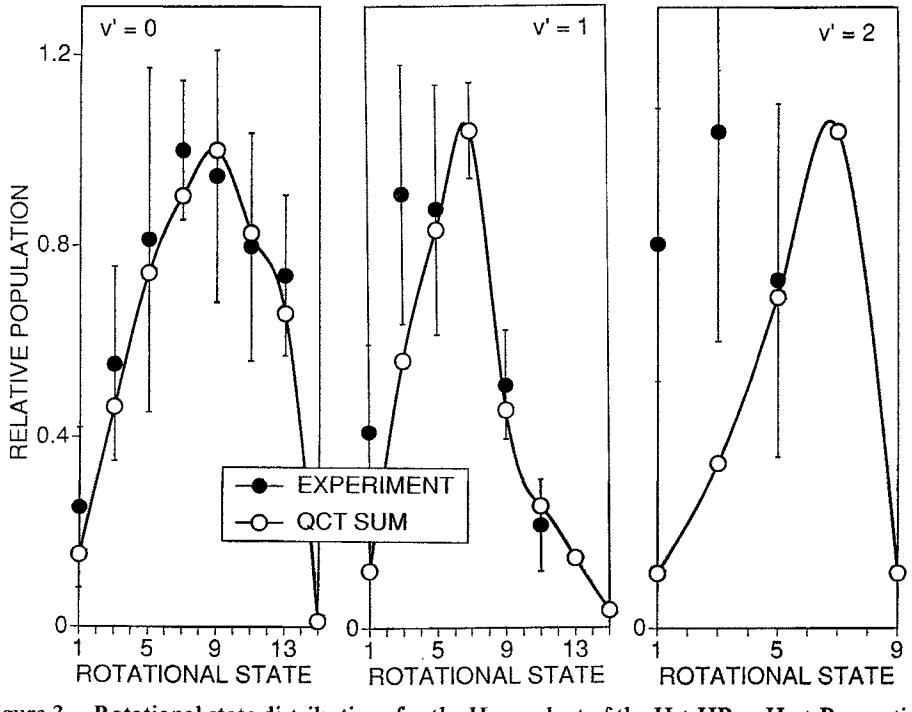

Figure 3. Rotational state distributions for the H_2 product of the $H + HBr \rightarrow H_2 + Br$ reaction at 1·6 eV collision energy.

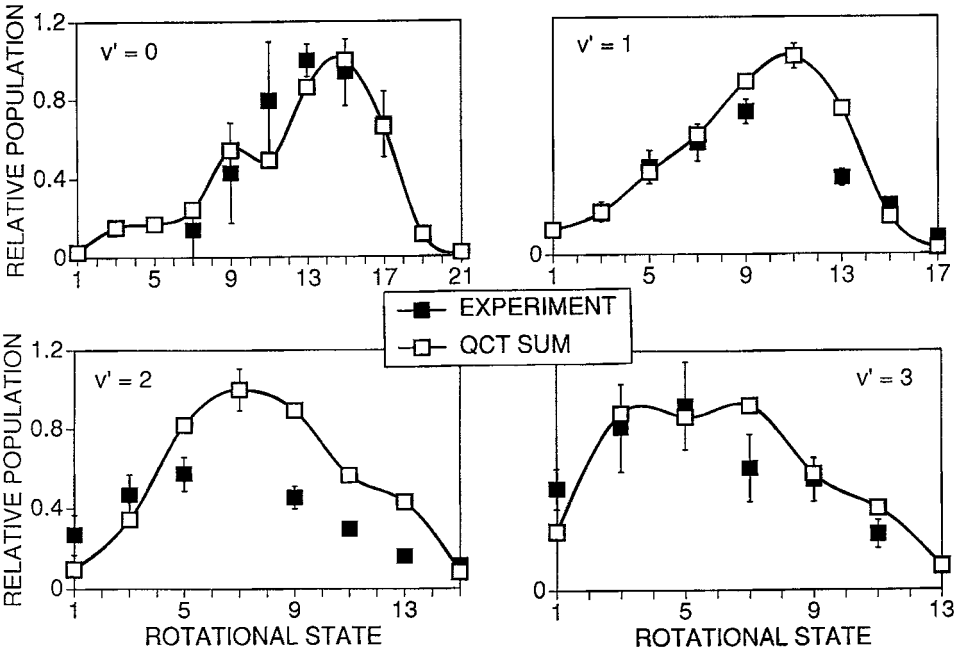

Figure 4. Rotational state distributions for the H_2 product of the $H+HI \rightarrow H_2+I$ reaction at 1·6 eV collision energy.

that reflects the steepness and position of the inner corner of the potential energy surface. The $H+HX \rightarrow H_2+X$ potential energy surfaces (Baer and Last 1981, Schwenke *et al.* 1989) dictate that the H–H distance at the turning point will not be much smaller than the equilibrium value for the H + HCl reaction, so the H_2 from this reaction should not be very excited vibrationally. In contrast, for the H + HBr and H + HI reactions, the H–H distances at the inner corner of the potential energy surface, where the Franck–Condon transition was postulated to occur, are much smaller, small enough that vibrationally excited H_2 should be common for $H+HBr \rightarrow H_2+Br$ and dominant for $H+HI \rightarrow H_2+I$.

We argued that this Frank–Condon (sudden) transformation of $H+HX$ into H_2+X would be followed by vibrationally adiabatic, rotationally impulsive energy release in the half-collision of H_2+X separation, by analogy with the behaviour often observed in photodiscussion, where a half-collision of products occurs from a steeply repulsive part of a potential energy surface. The implication of such a model is that product rotational excitation would be determined only by the available energy and the HHX geometry at the turning point. Using HHX bend potentials estimated by line-of-centres calculations, the impulsive model was used to predict peaks in, and shapes of, the H_2 product rotational state distributions. The predictions matched quite well the experimentally observed rotational energy disposal.

A comforting agreement perhaps, but this model inferred from just the experimental state-to-state measurements is untestable and does not extract as much information from the experimental measurements as is actually contained in them. For a complete picture of the reaction dynamics, it would be necessary to perform more detailed theoretical calculations. We thus modelled these reactions using the QCT formalism (Aker and Valentini 1990, Aker *et al.* 1992). The results of our QCT

calculations show that the Franck–Condon vibrationally adiabatic, rotationally impulsive model of $H + HX$ abstraction dynamics is incorrect. The calculations show that vibrational energy disposal is determined by the location of the potential energy surface saddle point, pretty much as one finds for reactive collisions at low collision energy. The rotational energy disposal in contrast is governed in large measure by kinematic and geometric constraints.

The derivation of detailed dynamical information from the QCT calculations requires that we first establish the validity and accuracy of the calculations for describing the real $H + HX + H_2 + X$ reactions. This we do by comparing the $H_2(v',j')$ state distributions from the QCT calculations with the corresponding experimental quantities. The computed rotational distributions match, almost perfectly, the distributions measured in the experiments. In figures 2–4, where we present the experimental results, we have also plotted the QCT rotational state distributions, and the good agreement is readily apparent. Within the combined errors (vertical bars representing 2σ confidence limits), there is almost perfect agreement. Figure 4 shows QCT results computed on the LEPS surface, but the DIM-3C results are essentially indistinguishable.

The theory–experiment agreement for the vibrational state distributions, while not perfect, is also quite good. Comparison of the experimental and theoretical $P(v')$ in figure 1 shows that the only significant difference between theory and experiment is that experiment shows vibrational population inversion between $v'=1$ and $v'=0$ for $H + HI \rightarrow H_2 + I$, while the QCT results do not.

That such good agreement is achieved between experiment and theory is not trivial. Only a small fraction of the energetically allowed product states are significantly populated by the reactions, so the reaction dynamics are quite selective. Theory predicts that all these, but only these, experimentally observed states should be appreciably populated. The calculations must contain the correct dynamics. In fact, we will consider the QCT calculations verified by the good agreement with experiment, and proceed to use them to explore aspects of the dynamics not accessible experimentally.

One of the interesting observations to come from this exploration is that some striking kinematic and geometric constraints are very important in the dynamics of these $H + HX + H_2 + X$ reactions. To extract these let us look at some correlations between parameters describing the reactive trajectories. The first correlation is between impact parameter, b, and input angle, θ. We define the input angle as the angle between the initial approaching H atom velocity vector and the H–X bond; $\theta = 0°$ corresponds to collinear H–X–H approach while $\theta = 180°$ is collinear H–H–X approach. Figure 5 presents scatter plots in which each point tells us the b and θ for a particular reactive trajectory. Results for all three reactions are shown. The H + HI results are those using the LEPS surface; we will not present results on the DIM-3C surface as the dynamical behaviour observed is identical with that for the LEPS H + HI surface.

All three plots show that there is a strong correlation between b and θ, that is that reaction can occur for a particular b only for a narrow range of θ and vice versa. Trajectories with small b lead to abstraction only if there is near collinear H–H–X approach geometry (i.e. $\theta = 180°$). If b is large, abstraction will occur only if approach geometry is perpendicular H–H–X (i.e. $\theta = 90°$). Quantitative analysis of this correlation shows that for reaction to occur the HX molecule must be oriented so that the approaching H atom either strikes the H atom on the HX directly, or comes within some small distance of it. A visual description of this situation is given in figure 6. What

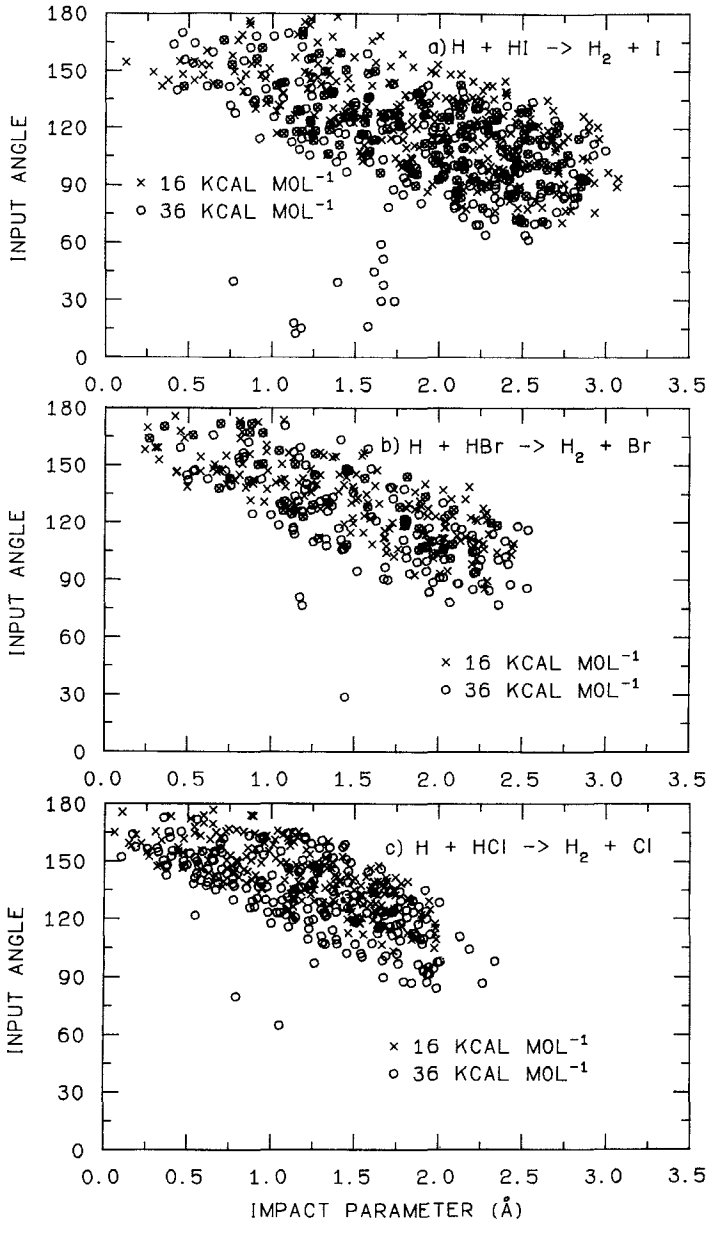

Figure 5. Scatter plots of the impact parameter versus H–H–X angle for reactive trajectories in $H+HX \rightarrow H_2+X$ at 1·6 eV (36 kcal mol^{-1}) and 0·7 eV (16 kcal mol^{-1}). From Aker and Valentini (1990).

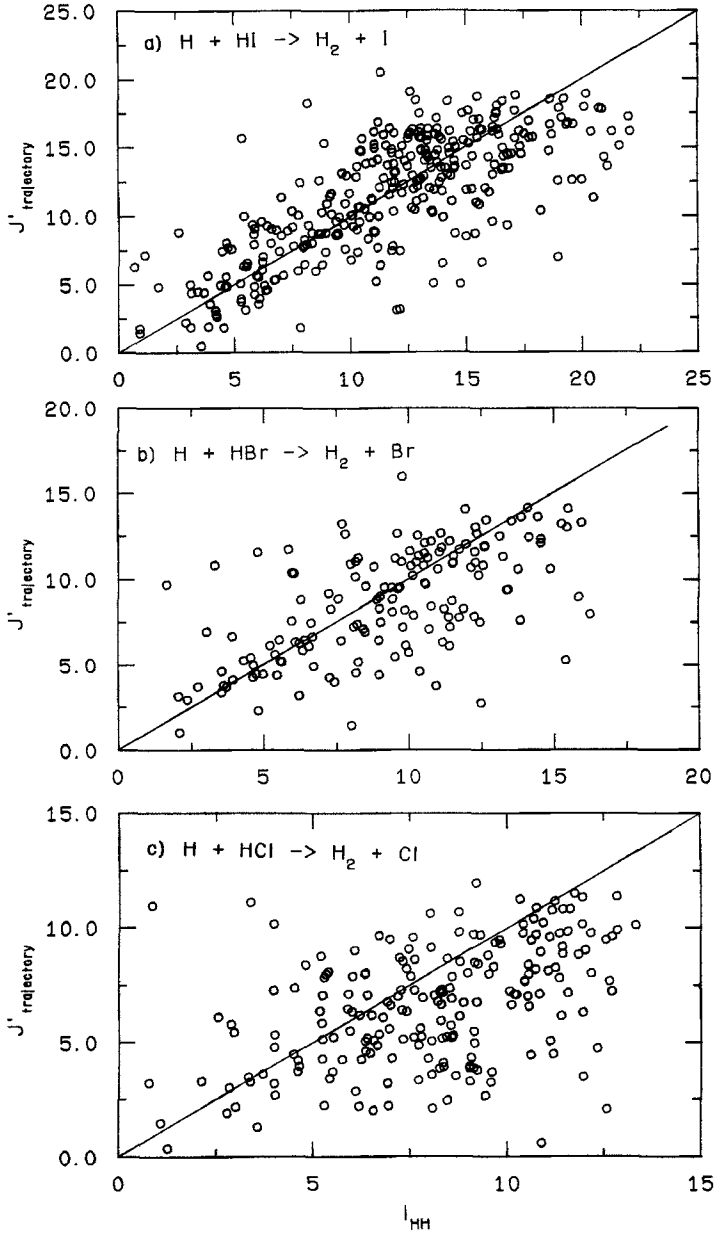

Figure 8. Scatter plots of the product rotational angular momentum versus H–H orbital angular momentum for reactive trajectories in $H + HX \rightarrow H_2 + X$ at 1·6 ev (36 kcal mol^{-1}). From Aker and Valentini (1990).

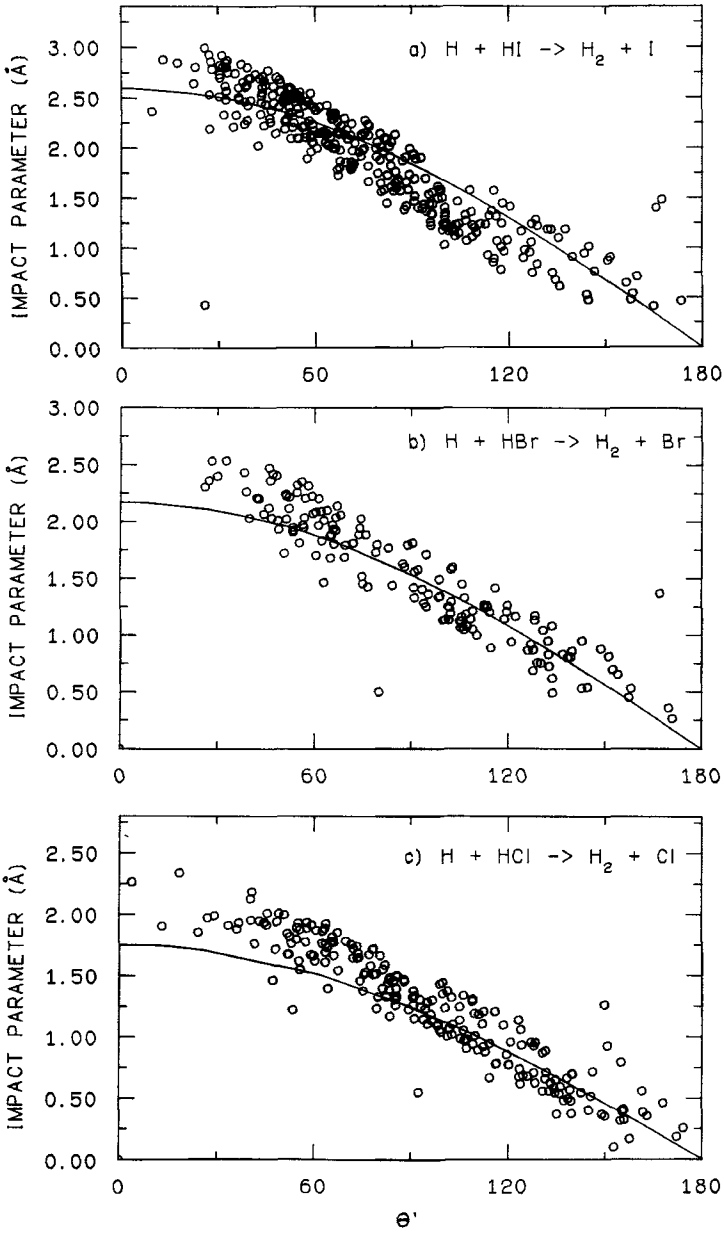

Figure 9. Scatter plots of the impact parameter versus product scattering angle for reactive trajectories in $H+HX \rightarrow H_2+X$ at 1·6 eV (36 kcal mol^{-1}). From Aker and Valentini (1990).

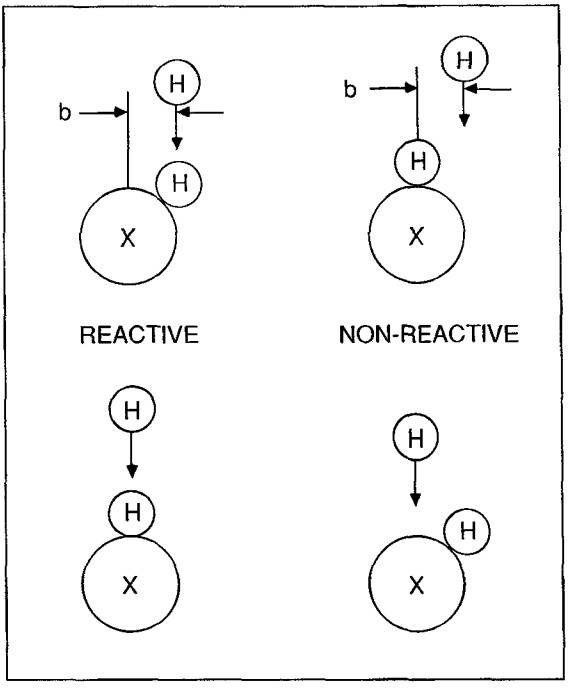

Figure 6. Schematic representation of the impact parameter-H–H–X angle correlation in the $H+HX \rightarrow H_2+X$ reactions.

we find is that the nominal impact parameter, so helpful generally in deciding whether two colliding species will react, is not useful at all for these reactions. Instead, the trajectory calculations suggest that we define a new impact parameter, measured not from the centre of mass of the HX, but rather from the centre of the H atom in the HX. Let us call this impact parameter b_{HH}; it is simply the distance between the attacking H atom velocity vector and a line drawn parallel to it that passes through the H atom located on the HX. The picture in figure 7 makes the definition clear.

Does the value of this impact parameter tell us anything about the outcome of the $H+HX$ collision besides whether reaction will occur? Yes. To see what let us look at another correlation from the trajectory results. Figure 8 shows another scatter plot, this time characterizing the reactive trajectories by their l_{HH}, j'. Here j' is the H_2 product rotational angular momentum and l_{HH} is the reactant orbital angular momentum of the H motion relative to H in HX. Note that $l_{HH}=\mu_{HH}v_{rel}b_{HH}$. We see that there is a very strong correlation between l_{HH} and j' for the reactive trajectories: $l_{HH}\approx j'$. This implies that the angular momentum of the H–H relative motion is conserved during the course of the collision, so the reactant orbital angular momentum, l_{HH}, is transformed into product rotational angular momentum, j'.

The correlation between l_{HH} and j' is not perfect. We could not expect it to be, since perfect correlation would imply that the halogen atom X is a spectator in the reaction. It is not, as the scatter plot of figure 9 shows. This is a plot of the pair b, θ' for the reactive trajectories. Here θ' is the scattering angle, the angle of recoil of the H_2 product relative to the velocity vector of the $H+HX$ approach. The correlation of b and θ' reveals the deflection function for the reactions, which follows the behaviour expected for hard-sphere scattering of H_2 from X. The solid lines in figure 9 are deflection functions

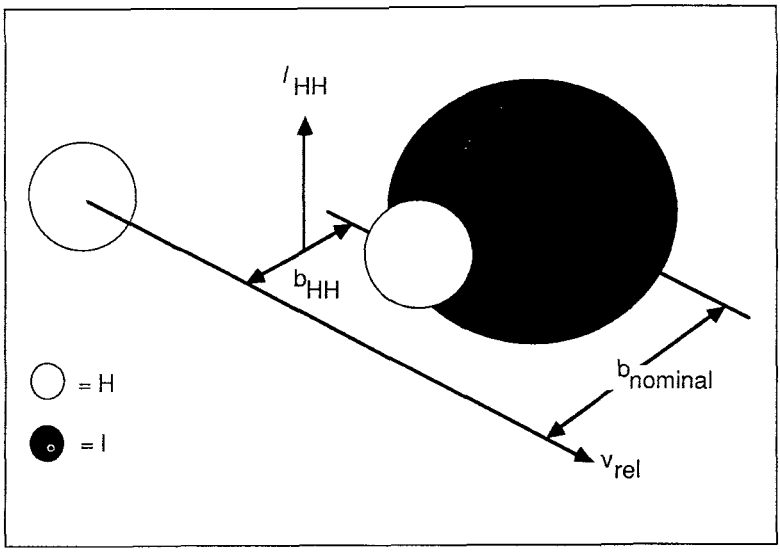

Figure 7. Diagram showing the relation between the nominal impact parameter, $b_{nominal}$, and the H–H impact parameter, b_{HH} in H + HX collisions.

calculated using hard-sphere collision radii given by the sum of the H–X bond distance plus one half the H–H separation at the saddle point on the surface of interest, and correspond to hard-sphere scattering of H_2 from X. The halogen atom cannot be a spectator in the reaction because it is too large to avoid colliding with the H_2.

The description of the high collision energy abstraction reaction dynamics as an isolated interaction between the two hydrogen atoms in the system with subsequent scattering of the newly formed H_2 off a large halogen atom helps explain why the cross-sections for abstraction are so small, even though the collision energy is substantially above the barrier height. The QCT cross-sections for the H + HI → H_2 + I reaction is 2·0(1) Å^2 on the LEPS surface and 1·8(1) Å^2 on the DIM-3C, while for H + HBr and H + HCl the abstraction reactions have cross-sections of only 0·8(1) and 0·39(3) Å^2. The experimental values are 1·1(3), 1·9(5), and 1·4(2) Å^2, for H + HCl, H + HBr, and H + HI, respectively. Although not in exact quantitative agreement the calculated and experimental cross-sections both indicate reaction cross-sections far smaller than hard-sphere gas kinetic values, despite the high collision energy.

The trajectories show why this is so: simple geometric constraints limit the abstraction reaction cross-section. As we have already discussed, the correlation between impact parameter and H–H–X angle (figure 5) shows that the incoming H atom must come within some critical distance of the H atom on the HX if reaction is to occur. We can calculate how this constraint limits the reaction cross-section by developing a geometric model based on it. We assume that reaction will occur if the impact parameter b_{HH} is less than the H–H distance at the saddle point of the potential energy surface. The probability that this condition will be satisfied for a particular value of the nominal (conventional) impact parameter, b, is given by the probability that the HX will be oriented to satisfy it (see figure 6).

This probability can be simply computed by representing the H atom distribution of orientations as a shell around the X, as shown in figure 10. The shell has an inner radius equal to the H–X bond distance at the saddle point and an outer radius equal to

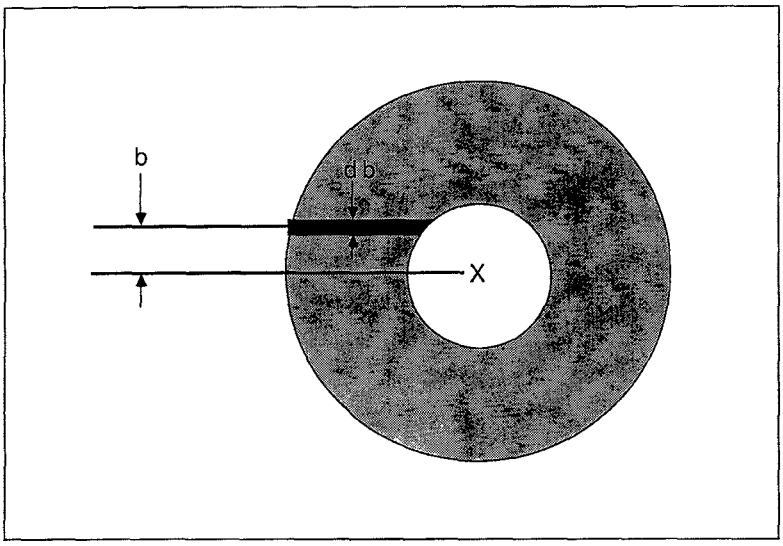

Figure 10. Schematic representation of HX used in the shell model of the $H+HX \rightarrow H_2+X$ reactions.

the sum of the H–X bond distance and the H–H distance at the saddle point. The zone of reactivity is then an annulus of radius equal to the H–H distance at the saddle point, and the probability of reaction at impact parameter b is just equal to the fraction of the volume of this annulus swept out at impact parameter b. This is purely a geometric reaction probability. Implicit in this model is the assumption that the collision is sufficiently energetic to allow reaction for any H–H–X geometry; as long as the H–H come within the critical distance reaction will occur.

The $H+HX \rightarrow H_2+X$ opacity functions, the probability of reaction at impact parameter b, calculated using this simple formalism are shown in figure 11. Also shown in this figure are the opacity functions actually determined in the QCT calculations for 1·6 eV collision energy. There is pretty good agreement between the two functions, in overall shape, in the value of the maximum b for which reaction occurs, and in absolute magnitude. There is also good agreement between the QCT and shell model calculated total cross-sections. The latter values are 1·7, 0·8, and 0·4 Å^2, for $X=$I, Br, and Cl, respectively. The general agreement of the shell model opacity function and the actual QCT opacity function shows that geometric effects dominate in determining the reaction probability. The small value of the reaction probability for any b, and hence the small total cross-section, is the result of the low probability of finding the H of HX in the right position for reaction—a consequence of the small size of H compared to X.

The picture that emerges here is of a reaction occurring as a transition from H + HX to H_2+X, not a small H–H and H–X distances as we originally proposed in the Franck–Condon model, but rather much earlier in the collision. The angular momentum in the H_2 product is thus largely determined by the H–H relative motion, that is by l_{HH}, and the vibrational state distribution mostly by the location of the reaction barrier.

The vibrational state distribution we determined experimentally for $H+HI \rightarrow H_2+I$ does not agree perfectly with the QCT results (see figure 1); the experiments show a population inversion between $v'=0$ and $v'=1$, while the calculations do not. Even for

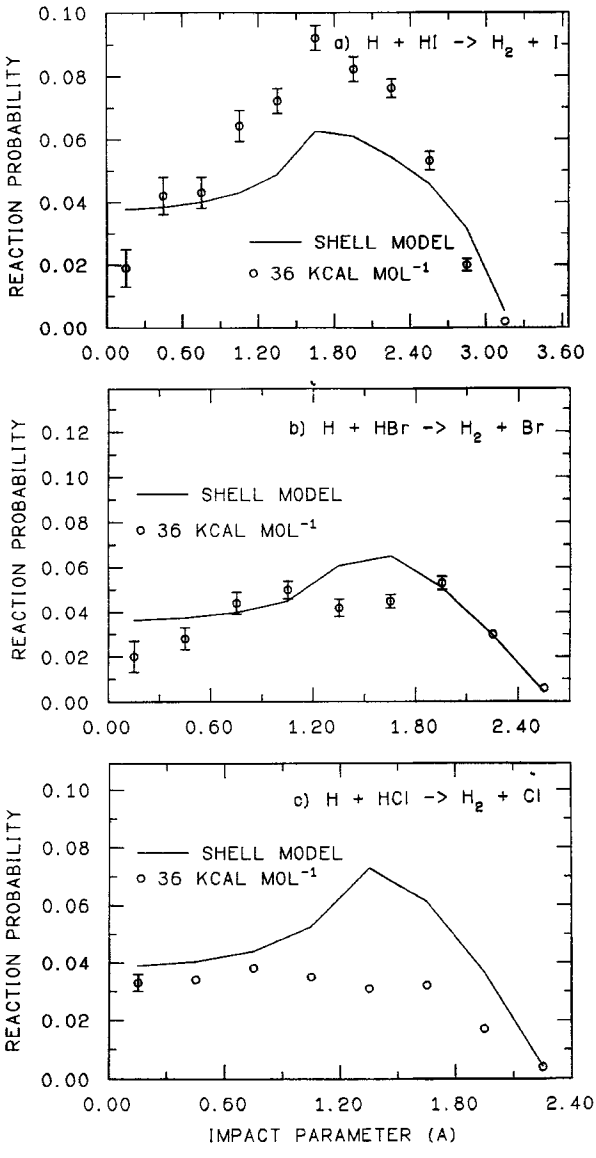

Figure 11. Comparison of QCT-calculated and shell-model-predicted opacity functions for the $H+HX \rightarrow H_2+X$ reactions at 1·6 eV (36 kcal mol^{-1}) relative energy. From Aker and Valentini (1990).

the $H+HBr \rightarrow H_2+Br$ reaction the QCT vibrational distribution is a bit older than the experimental one. Since the dynamics of the reactions revealed here indicate that the location of the barrier in the reaction is controlling the product vibrational distribution, this experiment–theory discrepancy suggests that the barrier for the $H+HI$ reaction needs to be moved a little. In fact, the trajectories provide direct evidence for this. A comparison of vibrational energy disposal in the QCT calculations at energies from 0·7 eV to 1·6 eV collision energy shows that the vibrational distributions become hotter as the collision energy is reduced. Since a reduction in collision energy has the same effect as making the potential surface less attractive, we

suggest that the H + HBr, and H + HI potential energy surfaces could be improved simply by moving the saddle point to smaller H–H distance, i.e. shifting the barrier toward the products. In fact, QCT calculations by González (González and Sayós 1989, González 1991) using an H + HI LEPS potential surface with an H–H saddle point distance much smaller than the saddle point distance on the LEPS surface we used yield a vibrational distribution that is very much like the one we observe experimentally in the 1·6 eV (nominal) collision energy $H + HI \rightarrow H_2 + I$ experiments.

4. $H + HX \rightarrow HX + H(X = Cl, Br, I)$

The careful reader will note that the heading for this section has a notation that differs from that used in our list of H + H*X* reactions (equations (1–3)) in Section 2. Here we do not distinguish between the exchange reaction, $H' + HX(v, j) \rightarrow H'X(v', j') + H$, and the non-reactive, inelastic energy transfer, $H' + HX(v, j) \rightarrow HX(v', j') + H'$. The removal of the distinction is deliberate. Experimentally we can distinguish these two channels only by isotopic substitution, e.g., using D + H*X* or H + D*X*. We attempted to do so in our experiments, using HI to generate the H atoms and DCl and DBr as the reactant diatoms. Unfortunately, isotopic scrambling between the HI and the DCl/DBr could not be sufficiently suppressed under the conditions of our experiments, and the presence of some DI in the HI and some HCl in the DCl (or HBr in the DBr) would make the experiments meaningless. Consequently, we have examined only the H + H*X* → H*X* + H isotopomer of the reaction and hence cannot separate the reactive exchange and inelastic energy transfer processes.

The rotational state distributions we measured (Aker *et al.* 1989)) for products in $v' = 0$ and $v' = 1$ for all three systems are presented in figures 12 and 13. The collision energy is nominally 1·6 eV, but as discussed in Section 2 the production of 1·6 eV H atoms by HI photolysis at 266 nm also yields some H atoms that give H + H*X* collisions with 0·7 eV collision energy. For each v' the data for the different systems are scaled such that the most populated j' level in each is assigned the value 1·0. Data for low j' levels in $v' = 0$ cannot be obtained, since the thermal population over j in the chemically identical reactant diatom and the small conversion of reactant to product in single-collision experiments preclude meaningful measurement at low j'.

For products in both vibrational states the H + HCl results differ measurably from those for H + HBr and H + HI, which are quite similar. The latter two systems give distributions extending to much higher j' than the former. For HI product in $v' = 0$ the maximum observed j' is 36 and the average value of j' is 20, while for $v' = 0$ HBr the maximum and average are 27 and 17. Compared on the basis of rotational energy rather than rotational angular momentum the similarities between H + HI and H + HBr are even more evident, since the differences in the average rotational angular momenta of the two products almost exactly offset the differences in rotational constant for the two molecules, 6·4 cm^{-1} for HI and 8·3 cm^{-1} for HBr. In contrast, for HCl in $v' = 0$ the maximum observed j' (17) and the average j'(11) are much lower, and the rotational energy imparted in the collision is only about half that in the collisions of H with HBr and HI. The same similarities between H + HI and H + HBr, and their difference compared with H + HCl are evident in the $v' = 1$ rotational state distributions, as the data in table 3 show. The differences cannot be due simply to larger average j in the thermal distribution of the reactants, since the most probable j of the reactants is nearly the same in all three systems, 3, 4, and 4 for HCl, HBr, and HI, as is the average value of j for each, 3·4, 4·0, and 4·5 respectively.

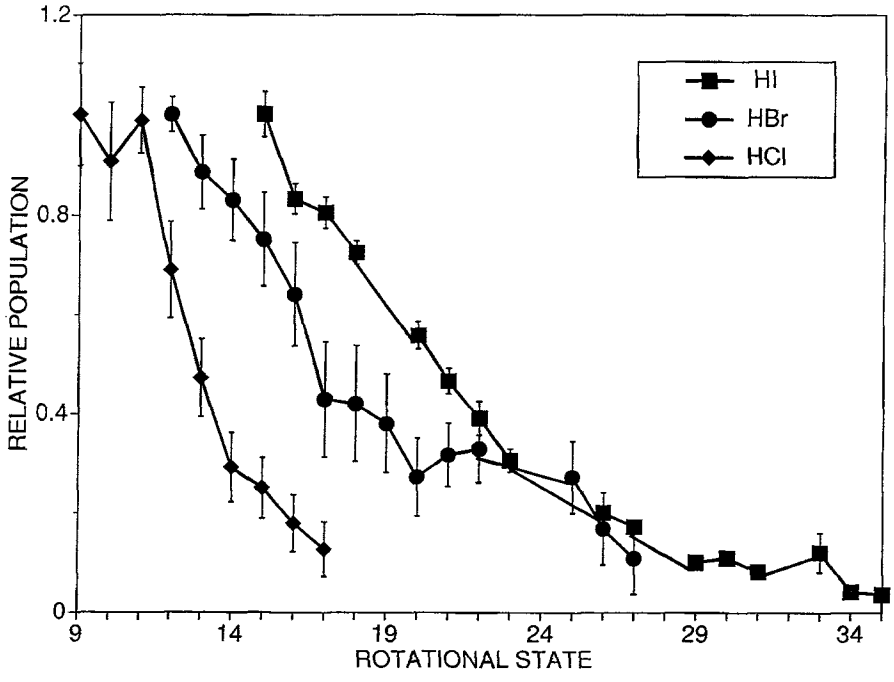

Figure 12. Rotational state distributions for the $v'=0$ HX product of $H+HX$ collisions at 1·6 eV relative energy.

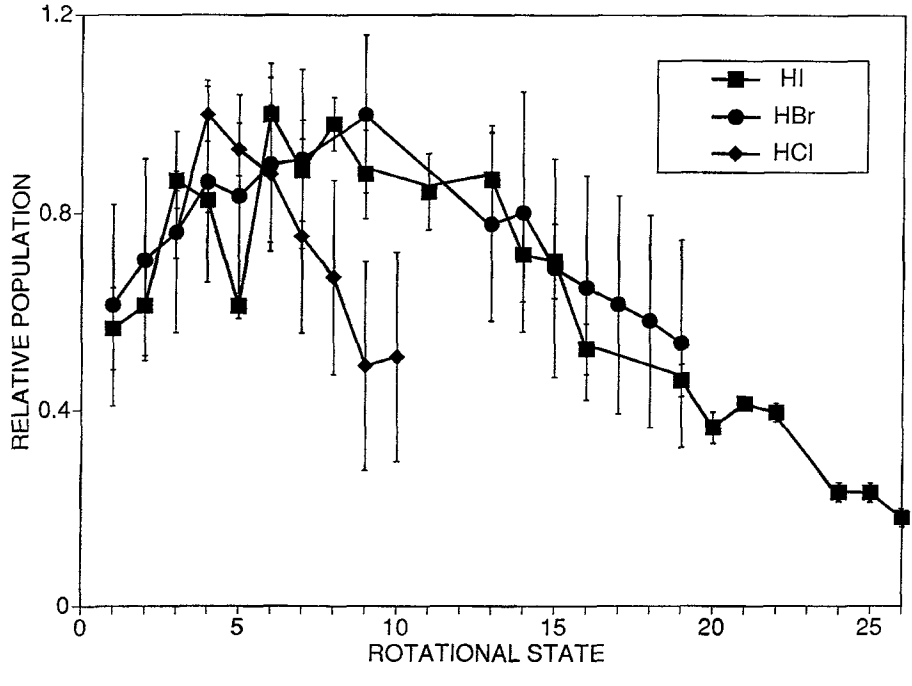

Figure 13. Rotational state distributions for the $v'=1$ HX product of $H+HX$ collisions at 1·6 eV relative energy.

Collisions of H with HI and HBr create quite highly excited rotational states. The HBr and HI product molecules with j' of 25 to 35 have rotational energies of 0·6 to 0·9 eV, representing one-third to one-half the collision energy. However, the average energy disposed in product rotation is much smaller, as the summary of the data in table 3 shows. Table 3 also presents a summary description of cross-sections and other characteristics of the three systems. One convenient summary of the rotational energy disposal for all three reactions that permits clear comparison among them is provided by a linear surprisal analysis of the data. This surprisal analysis (Levine and Bernstein, 1987) compares the actually observed rotational state distribution to that which would be observed if the collisions resulted in a statistical distribution over the energetically allowed energy levels, and represents the difference between the statistical and actual distributions by a single parameter. The surprisal parameter resulting from such an analysis is defined by the relation

$$P(j') = P^0(j') \exp - [\theta_R g_R(j')], \tag{4}$$

where $P(j')$ and $P^0(j')$ are, respectively, the experimentally observed rotational distribution and the statistical, so-called prior, distribution, and $g_R(j')$ is the fraction of the available energy that is contained in rotation for energy level j'.

The linear surprisal parameter θ_R conveys the deviation of the observed distribution from the statistical one, and thus measures the dynamical bias of the collision process. A positive rotational surprisal parameter, as we find for H + HCl, H + HBr, and H + HI shown in table 3, implies that the collision dynamics are biased against the deposition of energy in product rotation. Since the surprisal parameters characterize the rotational distribution of each system by comparison with the statisical distribution appropriate for that system, they reveal dynamical differences or similarities among the systems that cannot be obtained by simple comparison of the measured rotational state distributions.

The rotational surprisal parameters for all three $H + HX \rightarrow HX + H$ systems are large and positive, so each system shows dynamical bias against putting collision energy into product rotation. However, the surprisal parameter for H + HCl, $\theta_R = 15$, is twice as great as those for H + HBr ($\theta_R = 6{\cdot}8$) and H + HI ($\theta_R = 7{\cdot}6$). This indicates a pronounced difference between the H + HCl system and the other two: a bias against product rotational excitation in H + HCl that is twice as great as that in H + HBr and H + HI, which are quite similar to one another. This was a provocative difference, for in extensive studies of $H + D_2$ collisions at comparable collision energies we observed that inelastic collisions produced D_2 rotational state distributions characterized by surprisal parameters that were twice those for the reactive collisions producing HD (Gerrity and Valentini, 1984, 1985 a, b).

Table 3. Cross-sections and energy disposal in $H + HX \rightarrow HX + H$ collisions.

Parameter	HCl	HBr	HI
σ(Å^2)	13(3)	11(2)	11(2)
f'_v	0·02(1)	0·03(1)	0·02(1)
f'_r	0·06(2)	0·12(2)	0·11(2)
f'_t	0·92(3)	0·85(3)	0·87(3)
$\langle j' \rangle_{v'=0}$	20	17	11
$\langle j' \rangle_{v'=1}$	12	10	6
θ_r	15·4(8)	6·8(7)	7·6(5)

On the basis of all these differences between H + HCl on the one hand and H + HBr and H + HI on the other we speculated that H atom reactive exchange dominated the dynamics in the latter two systems, while inelastic energy transfer was predominant in the former. QCT calculations can of course distinguish the inelastic energy transfer and the reactive exchange even when the reactants and products are chemically identical, and so could be used to determine whether this speculation is correct. In fact, QCT calculations on H + HF inelastic energy transfer and reactive exchange at high collision energy had already been done by Schatz (1987) and showed that for $j=0$ reactive collisions the average j' was 2·5 times greater than the average j' characterizing the inelastic collisions.

We carried out QCT calculations on the H + HCl, H + HBr, and H + HI collisions at two relative energies, 1·6 eV and 0·7 eV, and combined the results in the proper proportions to reproduce the conditions under which the experiments were done. The trajectory calculations also used a 300 K Boltzmann distribution for the rotational state of the HX reactant. About 40 000 and 16 000 trajectories were run at 1·6 eV and 0·7 eV respectively. The maximum impact parameter of 5 Å produced full convergence of the results, even in the inelastic energy transfer channel.

The QCT and experimental results for the H + HCl reaction are compared in figures 14 and 15. The QCT cross-sections are divided into components for the inelastic energy transfer and for the reactive exchange. Note that this comparison is of absolute partial cross-sections, not simply relative state populations, and is thus a very stringent test of the theory. The agreement between the experiment and theory is generally quite good, but certainly not perfect. In $v'=1$ the QCT partial cross-sections have the correct magnitude, but show a somewhat broader distribution over j' than does the

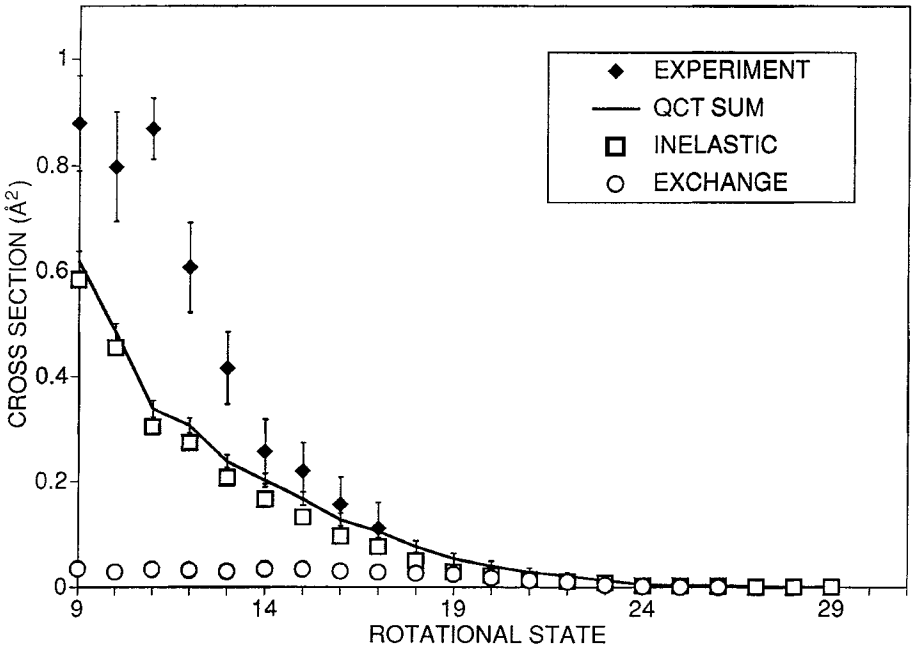

Figure 14. Comparison of experimental and QCT HCl ($v'=0,j'$) partial cross-sections from H + HCl → HCl + H collisions at 1·6 eV relative energy.

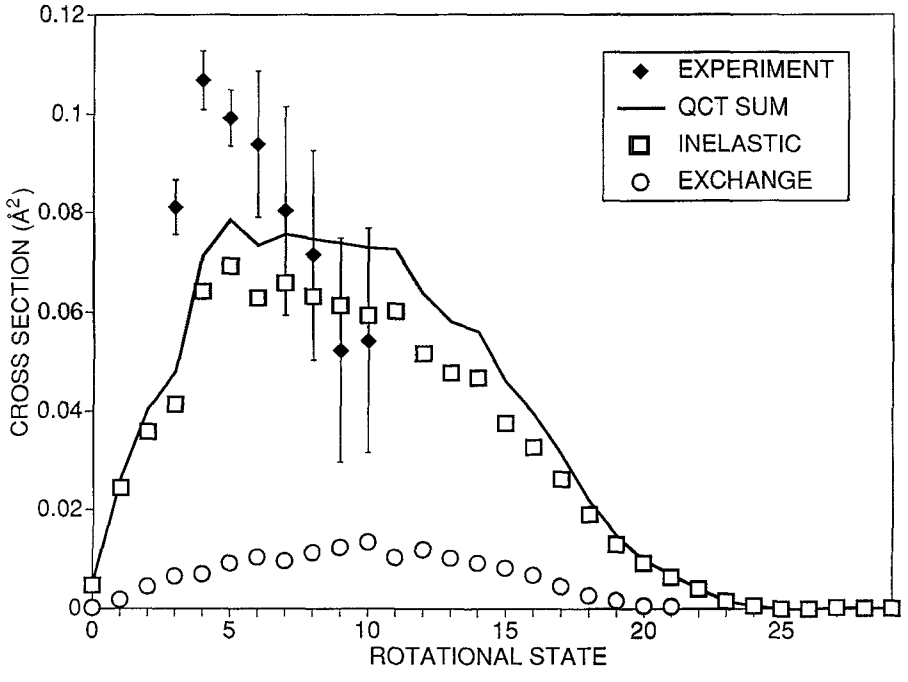

Figure 15. Comparison of experimental and QCT HCl ($v'=1, j'$) partial cross-sections from H + HCl → HCl + H collisions at 1·6 eV relative energy.

experiment. We must be careful about overstating the theory–experiment discrepancy here. The experimental measurements of the H + HCl $\sigma(v'=1, j')$ were right at the limit of the detectivity we had then. (The experimental sensitivity has since been improved by more than an order of magnitude, but these experiments have not been repeated or extended.) A partial cross-section of 0·05 Å^2 for HCl was about the smallest we could observe, so the absence of experimental data at small and large j' in $v'=1$ is not strong evidence for the absence of product in these states.

The absolute partial cross-sections for $v=0$ are a bit smaller in the calculations than in the experiments, but the overall shape of the distribution is quite good. This is emphasized by the plot in figure 16, in which we compare the QCT and experimental results for $v'=0$ after scaling them to have the same total cross-section. It is important to issue a caveat about theory–experiment comparison here as well. Production of the HCl in the lowest j' of $v'=0$ almost certainly is dominated by inelastic processes that sample the long-range part of the H + HCl potential. This is the hardest part of the potential energy surface to get accurately, since the interactions between the H and HCl are weak there. The H + HCl potential energy surface we use in our calculation was designed to describe the reactive, strong-collision encounters of H and HCl, not the large impact parameter, weak-interaction collisions.

Even though imperfect, the agreement between theory and experiment is certainly good enough to use the QCT results to conclude that in H + HCl → HCl + H collisions inelastic, not reactive, processes dominate in producing the HCl (v', j'). For both $v'=1$ and $v'=0$ product the trajectory results show much more product from the inelastic collisions than from reactive ones, except for the highest j' of $v'=0$, for which the cross-sections are very small.

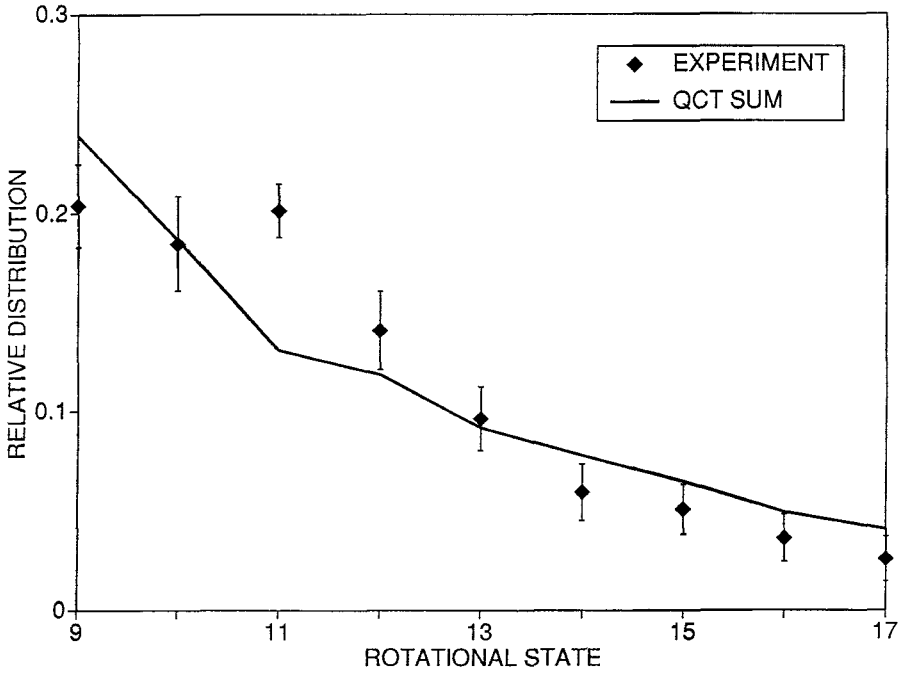

Figure 16. Comparison of experimental and QCT $v'=0$ HCl relative rotational state distributions from H+HCl→HCl+H collisions at 1·6 eV relative energy.

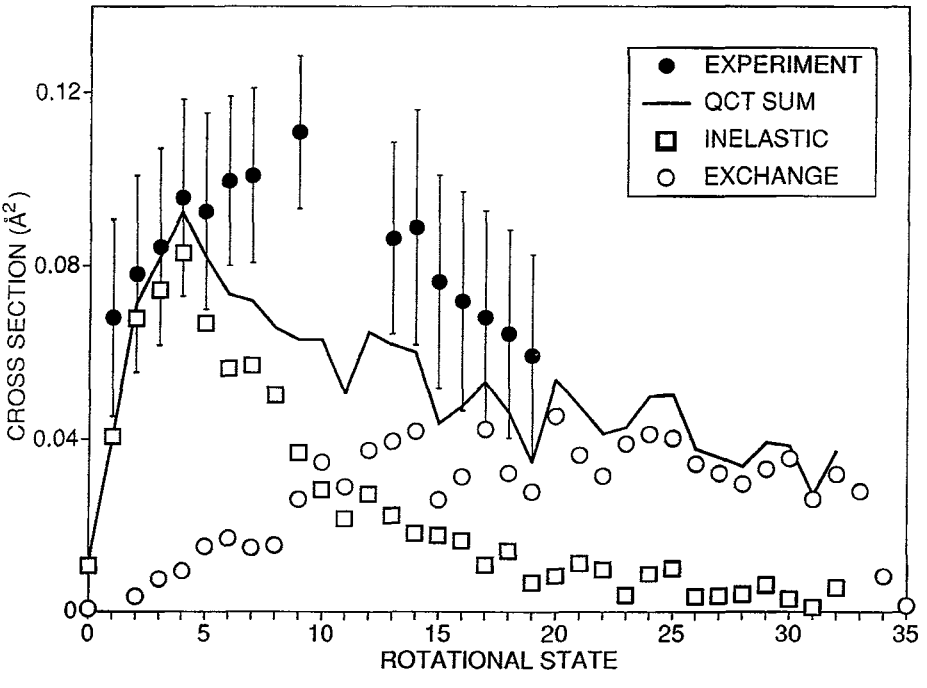

Figure 17. Comparison of experimental and QCT HBr($v'=1,j'$) partial cross-sections from H+HBr→HBr+H collisions at 1·6 eV relative energy.

What of the other two $H+HX \rightarrow HX+H$ systems? Figure 17 compares experimental and theoretical absolute $v'=1$ partial cross-sections for the H + HBr system, and shows that the agreement is quite good. For $v'=0$ (not shown) the experimental absolute partial cross-sections are about a factor of two larger than the QCT absolute cross-sections, but the shapes of the experimental and theoretical rotational distribution are very similar. The QCT calculations predict formation of HBr in $v'=2$, with a cross-section about 0·4 that of $v'=1$, and in $v'=3$ with a cross-section about 0·1 that of $v'=1$, while we observed no $v'=2$ or $v'=3$ in our experiments. However, the QCT-predicted $v'=2$ and $v'=3$ partial cross-sections are well below the experimental detection sensitivity, so this represents no discrepancy.

The agreement between theory and experiment is not so good and the experimental data with which to test the theory not so extensive as to give us confidence in using the calculations to develop detailed models of the collision dynamics. However, there is enough contact between experimental and QCT data and enough agreement where there is contact to convince us that the QCT data can resolve the contributions of inelastic and reactive exchange to the HBr (v', j') products. The decomposition of the HBr $(v'=1, j')$ cross-sections into inelastic and reactive contributions is given in figure 17. Both the inelastic and reactive processes contribute. For low j' the inelastic process is most important, while for high j' it is reactive exchange that dominates. For HBr $(v'=0, j')$ the behaviour is the same. So, the QCT results do confirm our original speculation that the reason that $H+HBr \rightarrow HBr+H$ collisions yield rotationally hotter products than $H+HCl \rightarrow HCl+H$ collisions is that only inelastic collisions are important in the latter while reactive exchange is important in the former. However,

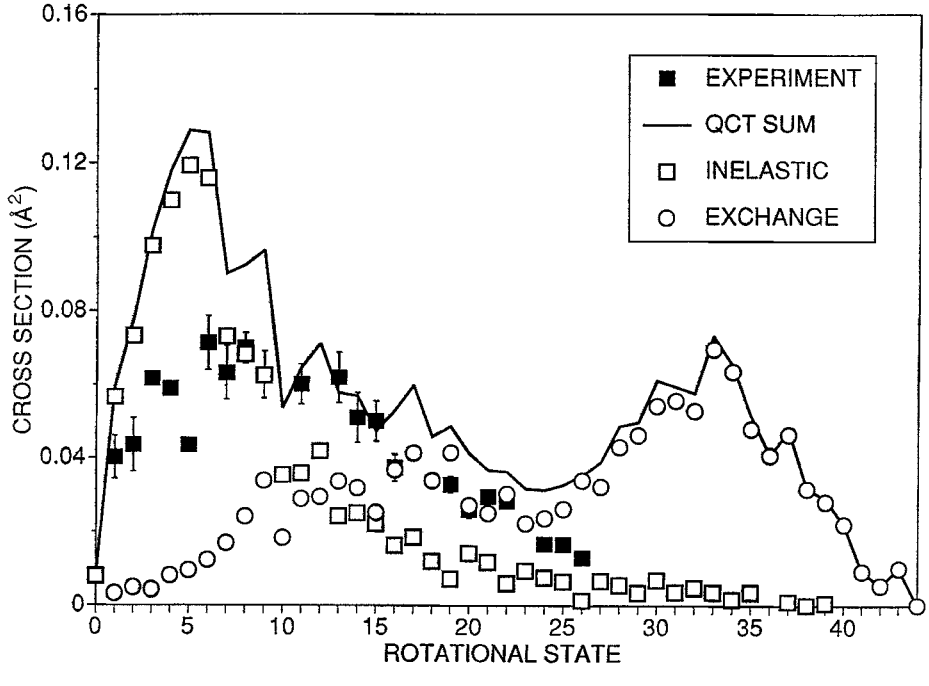

Figure 18. Comparison of experimental and QCT HI$(v'=1, j')$ partial cross-sections from $H+HI \rightarrow HI+H$ collisions at 1·6 eV relative energy. The QCT calculations use the LEPS potential energy surface of Parr and Kuppermann (1989).

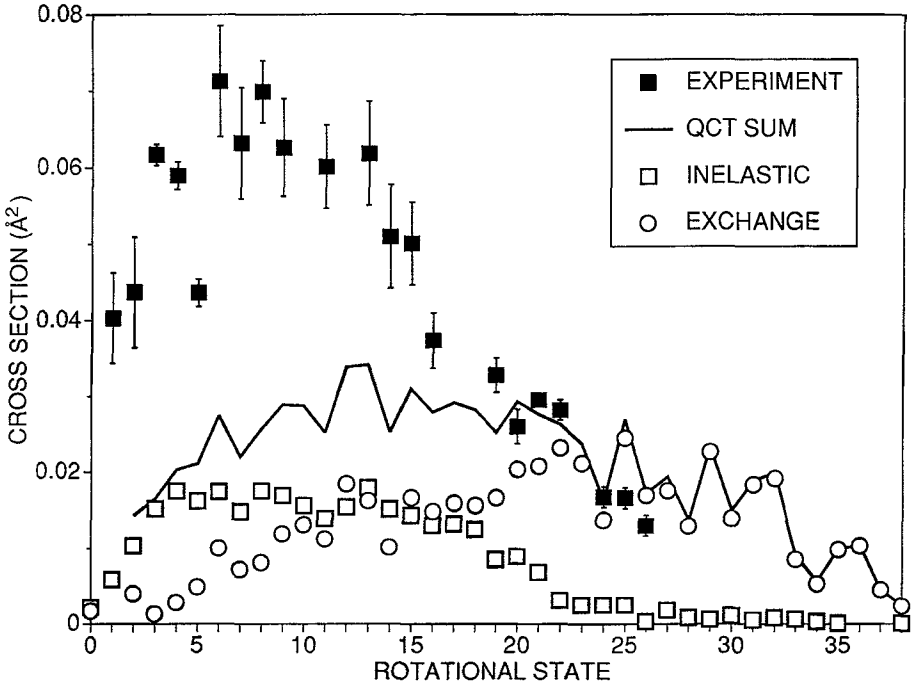

Figure 19. Comparison of experimental and QCT $v'=1$ HI partial cross-sections from H+HI→HI+H collisions at 1·6 eV relative energy. The QCT calculations use the DIM-3C potential energy surface of Baer and Last (1981).

our suspicion that reactive exchange dominates the H+HBr→HBr+H collisions is not borne out; the contributions are comparable.

The QCT results lead us to the same conclusions about the H+HI→HI+H collisions, although less convincingly. For H+HI the calculations do not agree with the experimental results well enough to make us confident about using them to elaborate the detailed collision dynamics. Comparison of QCT and experimental absolute partial cross-sections for H+HI→HI($v'=1,j'$)+H collisions are presented in figures 18 and 19. As we did when investigating the abstraction channel for H+HI collisions, we computed classical trajectories on two different potential energy surfaces, the LEPS surface of Parr and Kuppermann (1989) and the DIM-3C of Baer and Last (1981), Figure 18 plots QCT results using the former, and figure 19 the latter.

The result? Neither calculation gives results in good agreement with experiment. Rather, the experimental results lie somewhere between the theoretical results for the LEPS and DIM-3C surfaces. Calculations on both surfaces show comparable amounts of reactive exchange and inelastic energy transfer, but without good agreement of the calculations with the experiments, we are not justified in drawing conclusions about the collision dynamics from the QCT data.

We include this example here as a caveat to the reader. Not for every reaction system can we expect to find the wonderful convergence of QCT simulation and experimental measurement that allowed us to extract so much information about the dynamics of the $H+HX+H_2+X$ reactions. These are after all approximate calculations, and cannot be expected to be successful in every instance, no more than every experiment is successful. Of the components necessary to produce meaningful and

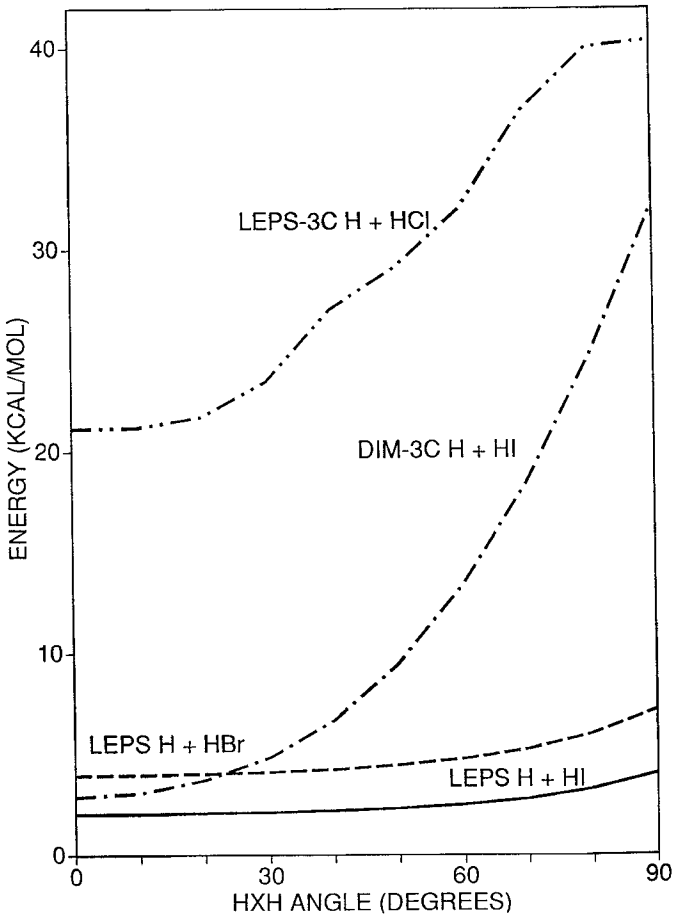

Figure 20. Plots of the potential energy surfaces along the H–X–H bend coordinate for the potentials used in the QCT calculations described here.

useful computational results, the one most likely to cause difficulties is the potential energy surface. The approximate nature of the surface is more often a limitation than the approximations attendant to the classical calculations.

To see how much of an uncertainty is in the approximate potential energy surfaces we show in figure 20 the angular part of the H + HX surfaces for the H–X–H geometry. Of note here is the pronounced difference between the DIM-3C and LEPS surfaces for H + HI. We would not expect these surfaces to give similar product state distributions for the H + HI → HI(v, j') + H collisions. Not surprisingly, the success of computational simulation of state-to-state reaction dynamics experiments depends on getting a good potential energy surface to work with.

5. Conclusions

QCT calculations on a variety of potential energy surfaces have been performed to model high energy H + HX (X = Cl, Br, and I) collisions. The results of these calculations, when used in conjunction with state-to-state experimental results, provide detailed pictures about the dynamics of these systems. This is an example of a fruitful interplay between theory and experiment.

Acknowledgments

This work is supported by the Division of Chemical Sciences, Office of Basic Energy Sciences, Office of Energy Research, U.S. Department of Energy.

References

AKER, P. M., GERMANN, G. J., TABOR, K. D., and VALENTINI, J. J., 1989, *J. chem. Phys.*, **90**, 4809.
AKER, P. M., GERMANN, G. J., and VALENTINI, J. J., 1989, *J. chem. Phys.*, **90**, 4795; 1992, *Ibid.*, **96**, 2756.
AKER, P. M., and VALENTINI, J. J., 1990, *Israel J. Chem.*, **30**, 157.
ARNOLDI, D., and WOLFRUM, J., 1976, *Ber. Bunsenges. phys. Chem.*, **80**, 892.
BAER, M., 1973, *Molec. Phys.*, **26**, 369.
BAER, M., and KOURI, D. J., 1972, *J. chem. Phys.*, **57**, 3441.
BAER, M., and LAST, I., 1981, *Potential Energy Surfaces and Dynamics Calculations*, edited by D. G. Truhlar (New York: Plenum).
BAUER, W., RUSIN, L. Y., and TOENNIES, J. P., 1978, *J. chem. Phys.*, **68**, 4490.
CADMAN, P., and POLANYI, J. C., 1968, *J. phys. Chem.*, **72**, 3715.
CADMAN, P., POLANYI, J. C., and SMITH, I. W. M., 1967, *J. chem. Phys.*, **64**, 111.
CLARY, D. C., 1989, private communications.
CLARY, D. C., and HENSHAW, J. P., 1986, *The Theory of Chemical Reaction Dynamics*, edited by D. C. Clary (Dordrecht: Reidel).
CLEAR, R. D., RILEY, S. J., and WILSON, K. R., 1975, *J. chem. Phys.*, **63**, 1340.
COUSINS, L. M., and LEONE, S. R., 1987, *J. chem. Phys.*, **86**, 6731.
GERRITY, D. P., and VALENTINI, J. J., 1984, *J. chem. Phys.*, **81**, 1298; 1985 *a*, *Ibid.*, **82**, 1323; 1985 *b*, *Ibid.*, **83**, 2207.
GONZÁLEZ, M., 1991, *J. chem. Soc. Faraday Disc.*, **92**, 339.
GONZÁLEZ, M., and SAYÓS, R., 1989, *Chem. Phys. Lett.*, **164**, 643.
KLINER, D. A. V., RINNEN, K.-D., BUNTINE, M. A., ADELMAN, D. E., and ZARE, R. N., 1991, *J. chem. Phys.*, **95**, 1663.
LEVENE, R. D., and BERNSTEIN, R. B., 1987, *Molecular Reaction Dynamics and Chemical Reactivity* (Oxford University Press).
MCDONALD, J. D., and HERSCHBACH, D. R., 1975, *J. chem. Phys.*, **62**, 4740.
MUCKERMAN, J. T., 1989, private communication.
PARR, C., and KUPPERMANN, A., 1989, private communication.
RAFF, L. M., and THOMSPON, D. L., 1985, *Theory of Chemical Reaction Dynamics*, Vol. III, edited by M. Baer (Boca Raton: CRC Press).
SCHATZ, G. C., 1987, *J. chem. Phys.*, **86**, 6738.
SCHATZ, G. C., and ROSS, J., 1977, *J. chem. Phys.*, **66**, 1021.
SCHMIEDI, R., DUGAN, H. MEIER, W., and WELGE, K. L., 1982, *Z. Phys. A*, **304**, 137.
SCHWENKE, D. W., TUCKER, S. C., STECKLER, R. BROWN, F. B., LYNN, G. C., TRUHLAR, D. G., and GARRETT, B. C., 1989, *J. chem. Phys.*, **90**, 3110.
TRUHLAR, D. G., and MUCKERMAN, J. T., 1979, *Atom–Molecule Collision Theory*, Vol. III, edited by R. B. Bernstain (New York: Plenum Press).
VALENTINI, J. J., 1985, *Spectrometric Techniques*, Vol. 4, edited by G. A. Vanasse (New York: Academic Press).
VAN DER ZANDE, W. J., ZHANG, R., ZARE, R. N., and VALENTINI, J. J., 1991, *J. phys. Chem.*, **95**, 8205.
WIGHT, C. A., MAGNOTTA, F., and LEONE, S. R., 1984, *J. chem. Phys.*, **81**, 3951.